Taylor-Weighting Ridge Gap Waveguide Feed Network for Low-Profile Fully Metallic Array Antennas

Damián Pla-Herliczka, Jose I. Herranz-Herruzo, *Member, IEEE*, Miguel Ferrando-Rocher, *Senior Member, IEEE*, and Alejandro Valero-Nogueira, *Senior Member, IEEE*

***Abstract*—This letter showcases advancements in metallic array antennas tailored for millimeter-wave (mm-Wave) applications, supported by novel highly compact unbalanced dividers conceived in ridge gap waveguide technology. This innovative approach streamlines the feeding network by enabling high-weight-ratio dividers without adding design complexity. The study presents an 8 × 8 Ka-band antenna array employing Taylor amplitude tapering and featuring a compact corporate-fed design that effectively mitigates coupling effects between the feeding network and radiating elements. Experimental results highlight promising characteristics, boasting a matching better than −10 dB across the entire band of interest [(29 to 31) GHz] and secondary lobes below −20 dB while achieving a radiation efficiency exceeding 82%.**

***Index Terms*—Corporate feeding network, gap waveguide (GW), high efficiency, Ka-band, metallic array antennas, ridge gap waveguide (RGW), single layer, Taylor amplitude tapering, unbalanced power dividers.**

I. Introduction

THE increasing demand for bandwidth in wireless communications has spurred the rapid development of satellite networks. A prevailing trend in the space sector is the deployment of numerous satellite constellations that allow for increasing user bandwidth [1], [2]. With the electromagnetic spectrum becoming more crowded, antennas for these links must meet various specifications, such as high efficiency, robust designs in hostile environments, compact size, or reduced sidelobes. Fully metallic antennas have a significant advantage over other types due to their high efficiency and power handling, mechanical robustness, and ease of design. Gap waveguide (GW), a technology with demonstrated potential [3], [4], [5], [6], has made significant advancements in the past decade and is presented as a good solution for these types of antennas. The nature of the technology brings numerous advantages, such as preventing field leakage, a common problem in waveguide (WG) arrays, or providing flexibility for manufacturing through milling or additive processes.

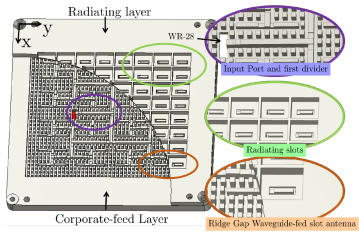

Fig. 1. Antenna schematic highlighting key components. Purple circle: input port and splitters. Green circle: slots. Orange circle: RGW feeding the slot.

In this context, antenna arrays with low sidelobe level (SLL) are highly sought after because they minimize interference. While various techniques are employed for SLL control, applying a specific amplitude distribution scheme to each array element is prevalent. In this context, the Taylor distribution [7] is a well-known and widely used option. The vast majority of works rely on substrate-based designs due to the maturity of printed circuit board (PCB) technology and its ease of design and production [8]. However, such arrays struggle with efficiency, power handling capability, and problems in harsh environments [9], [10]. Other works based on WG technology also address the SLL issue. However, WGs tend to be bulky and heavy or require several layers, and the manufacturing process often constrains the design [11], [12], [13], [14]. In the GW field, this specific amplitude distribution is usually achieved by designing appropriate corporate feeding networks [15], [16], [17], [18], [19]. In this approach, a careful design of the dividers plays the most crucial and sensitive role within the feeding network as they create the amplitude taper. Different types of dividers can be distinguished based on whether a ridge gap waveguide (RGW) or groove gap waveguide (GGW) is used. While the dividers proposed in the literature serve their purpose, they come with certain drawbacks, including high complexity, tolerance sensitivity, need for multiple layers, bulkiness, or a low weight ratio among the outputs.

This letter introduces a novel unbalanced divider design utilizing RGW technology for constructing corporate feeding networks with controlled amplitude tapering. Overcoming the limitations of prior designs, this compact and versatile divider allows easy control over the output ports' amplitude with a uniform phase, while enabling a straightforward manufacturing process. To substantiate the advantages of the proposed divider, an 8 × 8 RGW array antenna, seen in Fig. 1, has been experimentally

Manuscript received 19 April 2024; revised 21 May 2024; accepted 21 May 2024. Date of publication 24 May 2024; date of current version 6 September 2024. This work was supported in part by MCIN/AEI/ 10.13039/501100011033 under Grant PID2022-141055NB-C21 and in part by ERDF A way of making Europe, and the funding for open access was supported by the CRUE-Universitat Politècnica de València. *(Corresponding author: Miguel Ferrando-Rocher.)*

Damián Pla-Herliczka is with the Institut d'Electronique et des Technologies du numéRique (IETR), 35708 Rennes, France (e-mail: Damian.Pla-Herliczka@insa-rennes.fr).

Jose I. Herranz-Herruzo, Miguel Ferrando-Rocher, and Alejandro Valero-Nogueira are with the Department of Communications, Universitat Politècnica de València, 46022 Valencia, Spain (e-mail: jiherhe@upvnet.upv.es; miguel.ferrando@upv.es; avalero@dcom.upv.es).

Digital Object Identifier 10.1109/LAWP.2024.3404998

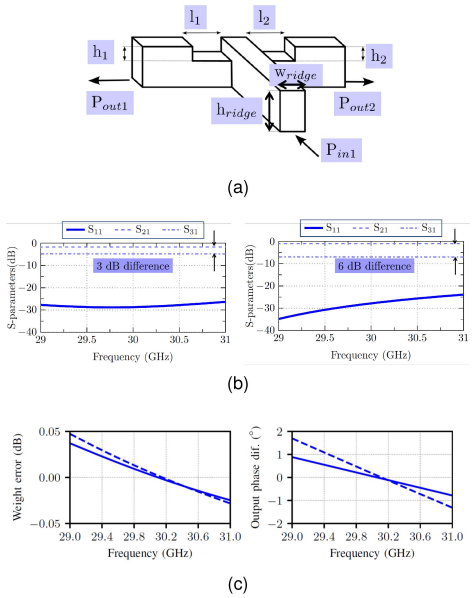

Fig. 2. (a) Schematic structure of the proposed RGW divider (ridge only). (b) S-parameters of 3 dB and 6 dB dividers. (c) Weight error and output phase difference of 3 dB and 6 dB dividers (solid and dashed lines, respectively).

validated. The feeding network, exclusively built with RGW, directly powers each radiator without requiring a coupling cavity, facilitating miniaturization with a single-layer approach. Experimental results confirm the antenna's high efficiency, significant improvements in SLL, and robust manufacturing characteristics.

II. RGW Dividers

Dividers are the most critical elements when designing corporate feeding networks for low sidelobe arrays. The topology used affects the space to be occupied, the coupling with adjacent network and radiating elements, and the overall performance of the divider. In a uniform array, every divider must distribute waves with the same amplitude and phase to each output, thus facilitating their design. In the case of unbalanced dividers, however, an asymmetry in the structure must be introduced to induce a power difference between the output ports. In GW technology, several unbalanced GGW dividers have been proposed [15], [16], [17], [20]. However, few solutions can be found in RGW technology, and they tend to be bulky and contain many tuning elements, significantly complicating corporate feeding network design. A higher number of tuning elements slows the optimization task, hinders the manufacturing process, and compromises the required fabrication tolerances. This work proposes the novel unbalanced RGW divider shown in Fig. 2(a). As can be seen, the structure is straightforward. Two notches at the top of the output ridges allow for control of the impedance and propagation constant, i.e., power ratio and phase delay, by only using four variables (l_1, l_2, h_1, and h_2). This fact significantly reduces the design complexity while providing the desired response in amplitude and phase. Obviously, in balanced dividers, both notches will be symmetrical. In the case of an unbalanced divider, the notches are designed independently with the help of an optimizer until the desired output weights are achieved. The proposed approach enables high output weight ratios with a seamless modification of a conventional splitter. One of its most appealing advantages is its natural ability to be integrated into the distribution network, avoiding tapers or pedestals. Moreover, thanks to such design simplicity, the construction is an additional advantage, allowing for the possibility of manufacturing with 3-D printing technologies.

TABLE I
(A) Dimensions of the BoN; (B) Dimensions of the 3 dB and 6 dB Dividers Shown in Fig. 2(A)

Variable	Size (mm)
Air gap	0.2
Nail height	2.5
Nail width$_x$	1.1
Nail width$_y$	1
Periodicity$_x$	2
Periodicity$_y$	1.9

(a)

Variable	Size (mm)	
	3 dB	6 dB
h_{ridge}	2.4	2.4
w_{ridge}	1.17	1.17
h_1	0.16	0.17
h_2	0.36	0.57
l_1	1.55	1.02
l_2	1.88	1.86

(b)

TABLE II
Performance Comparison With Different Dividers

Ref.	Weight-ratio (dB)	Max. phase diff. (°)	Return Loss (dB)	Size
[15]	2.68±1	*[1]	>20	Large
[13]	4.1±0.1	6.5	>30	Large
[16]	5±0.4	3	>17	Medium
[17]	5±0.9	4	>10	Large
[20]	6.7±[1]	7	>20	Large
This work	**3±0.03**	**0.9**	**>23**	**Small**
This work	**6±0.05**	**1.8**	**>25**	**Small**

[1] Value error unknown.

For example, Fig. 2(b) and (c) shows the performance of 3 dB and 6 dB unequal power dividers. The *S*-parameters, weight error in amplitude, and phase difference between outputs are depicted. These dividers exceed 35% bandwidth ($S_{11} \leq -10$ dB). However, only a fraction of this bandwidth will be used for antenna design, covering the (29 to 31) GHz SATCOM transmission band. As it can be seen, aside from the good matching level in both cases, the power ratio between outputs is easily attained, resulting in a very low drift, less than 0.03 and 0.05 dB (for the 3 dB and 6 dB dividers, respectively). Regarding the output phase difference, since the proposed dividers allow tuning the zero phase at the center of the band, the maximum phase drift is reduced, achieving very low phase differences between output ports ($0 \pm 0.8°$ and $0 \pm 1.7°$, for each divider). Table I contains the physical dimensions of the dividers and the bed of nails (BoN) where they are hosted. These pins' dimensions create an appropriate stopband, in which no mode propagates in our band of interest, from 29 GHz to 31 GHz.

Table II is provided for the sake of comparison with available dividers in the literature. It can be seen how, in all cases, the phase difference between output ports is 3° at best, while in the proposed designs, it is decreased to less than 0.9°, in the case of the 2:1 divider, and 1.8° for the 4:1 divider. In addition, the weight error is almost negligible, lower than 0.1 dB for both dividers, while compared to other cases, it can even reach 0.9 dB. These errors are negligible in arrays with a small number of radiating elements. However, in the case of large arrays, the phase and amplitude error is accumulated for each divider traversed, greatly increasing the effect on the final radiator. Therefore, the error produced in power weight and phase must be as small as possible.

III. Array Design

As an example of use, an 8 × 8 Ka-band array antenna with Taylor distribution has been designed. The corporate feeding network takes advantage of the above proposed dividers, allowing the design of a low-profile array that minimizes field

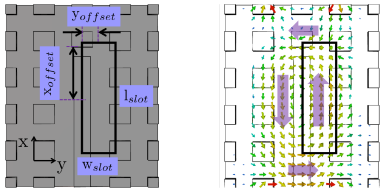

Fig. 3. H-field distribution in the unit cell at 30 GHz.

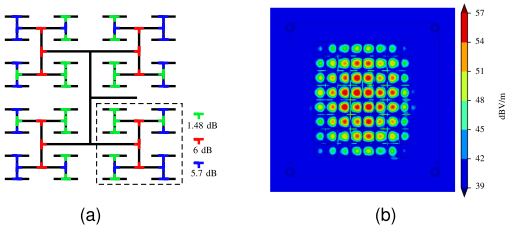

Fig. 4. (a) Weight ratios in the splitters and (b) E-field amplitude at 30 GHz.

coupling between the feeding network and the radiating elements. The 1×1 cell can be seen in Fig. 3. The array has a periodicity between unit cells of $0.8\lambda_0 \times 0.95\lambda_0$. Each output of the corporate feeding network feeds an open-ended ridge, which couples to an offset rectangular slot radiating into free space.

In a ridge WG, while the electric field maximum occurs at the center of the ridge, the longitudinal magnetic field has a component in the direction of propagation (x-axis in Fig. 3) which is maximum along the sides of the WG. Placing a slot parallel to this longitudinal direction allows the H-field to couple to the slot and produce efficient radiation. The slot dimensions, its distance to the ridge end, the offset from the center of the ridge, and the ridge height (l_{slot}, w_{slot}, x_{offset}, y_{offset}, and h_{ridge}, respectively) are optimized to maximize both bandwidth and matching values. The slot's length tends to be around $\lambda_0/2$, while the distance to the WG short, x_{offset}, is around $\lambda_0/4$ to maximize the field coupling. In this regard, it is noteworthy that if the ridge is close to the cover, the field will mostly be confined within the ridge width, making slot excitation much more difficult. Hence, optimizing the ridge height enables an effective magnetic field coupling to the slot for wideband free space radiation. Regarding the slot array lid, it is typical to introduce a waffle shape surrounding the slots to give the structure more rigidity and avoid material stress that could bend the metallic piece. It also acts as an interface between the slot and the free space, improving matching. Since the slot is not centered in the unit cell (see Fig. 3), the same offset has been applied to the cover waffle to avoid any asymmetry in the radiation pattern.

The corporate Taylor feeding network has been designed for a nominal SLL of 25 dB in both x- and y-planes, resulting in three different values of weight ratios: 6 dB, 5.7 dB, and 1.46 dB. The distribution of these dividers along the feeding network can be seen in Fig. 4(a). Within the network, spanning from the input port to each radiating element, the field passes through six dividers in total. They are sequentially numbered, with first denoting the splitter immediately after the input port and the sixth positioned closest to the radiating slot. The resulting electric field at the design frequency across the array aperture can be seen in Fig. 4(b), where the amplitude tapering toward array edges is evident.

It is important to note that the ridge height along the entire corporate feeding network differs from that of the unit cell. Its height, h_{R2}, is 2.4 mm, greater than the ridge of the unit cell, h_{R1}=1.77 mm. Fig. 5 illustrates the field distribution along a

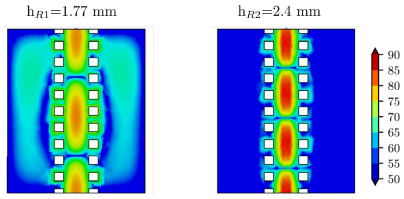

Fig. 5. E-field distribution of a section of an RGW with different ridge heights.

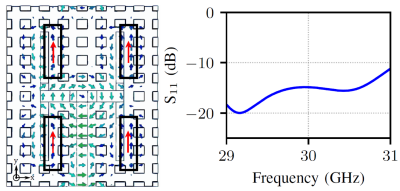

Fig. 6. H-field at 30 GHz and S_{11} parameter of the 2×2 cell.

Fig. 7. Manufactured prototype. (a) Cover slipped and (b) full assembly.

RGW for these two heights, surrounded by 1 row of pins. It is observable that the ridge with a height of 1.77 mm results in appreciable field leakage, potentially impacting the nearby elements within the feeding network. Specifically, this reduced height in the 2×2 unit cell enables the field to couple to the slot. Conversely, a height of 2.4 mm concentrates the field in the upper ridge, significantly reducing field leakage effects across the first stages of the network.

Considering that the ridge height for the radiating slots differs from that of the network, a stepped transition is employed to align these varying heights. The optimal placement for this transition is situated as close as possible to the radiating element, maximizing field confinement along the feeding network. Due to the compact nature of the network, there is limited space to position the transition immediately after the sixth-level divider or between the fifth and sixth-level dividers. Consequently, the transition is ultimately positioned right after the fourth-level divider. Note that this distinction is pivotal for the design's functionality and is advantageous. The cell combines unbalanced dividers with the high-to-low ridge transition, aiming to mitigate potential coupling effects from the proximity of slots, dividers, and transition components. This is demonstrated by the field behavior within the 2×2 unit cell, shown in Fig. 6. Despite minor leakiness, the magnetic field excites in phase the four slots, exhibiting a good reflection coefficient.

IV. Experimental Results

The designed array has been fabricated using computer numerical control (CNC) machining. The resulting antenna covers a total surface area of 100 mm $\times$ 100 mm and only 9.7 mm height (equivalent to $10\lambda_0 \times 10\lambda_0 \times 0.97\lambda_0$). Fig. 7 corresponds to the photographs of the manufactured prototype. Fig. 8 illustrates the measured and simulated matching at the input port. The reflection coefficient exhibits a consistent value lower than -10 dB across a bandwidth extending from 28.4 GHz to 31.7 GHz. The range for the intended application from 29

TABLE III
COMPARISON TABLE WITH LOW SLL ARRAY ANTENNAS IN THE LITERATURE

Ref.	Full-metal	Band	BW (%)	Rad. Eff. (%)	SLL (dB)	Technology	N° pieces	Dimensions (λ_0)
[11]	Yes	K_u	13.8	70	-24.1	Hollow Waveguide	4	$12.18 \times 12.18 \times 0.9$
[14]	Yes	E	19.2	70	-21	Hollow Waveguide	3	$8.4 \times 8.4 \times 1.84$
[15]	No	K_a	16	42	-18	Printed GW	4	$6.4 \times 6.4 \times 0.17$
[16]	Yes	W	5.7	74	-19.7	Gap Waveguide	3	$>10.72 \times 11.16\times^*$
[17]	Yes	K_a	5	40	-18.5	Gap Waveguide	3	$11.2 \times 11.2\times^*$
[21]	No	K_a	33	30	-13	Substrate Integrated GW	3	$6.50 \times 6.50 \times 1$
[22]	No	V	18.5	50	-23	Inverted microstrip GW	4	$13.18 \times 13.18\times^*$
[23]	Yes	X	0.34	30	-28.8	Slotted Waveguide	3	$7.27 \times 7.27\times^*$
This work	**Yes**	**K_a**	**10.98**	**82**	**-21**	**Gap Waveguide**	**2**	$\mathbf{10 \times 10 \times 0.97}$

BW: -10 dB impedance bandwidth; Rad. Eff.: Total Radiation Efficiency as defined by IEEE Standard [24].
*: No information.

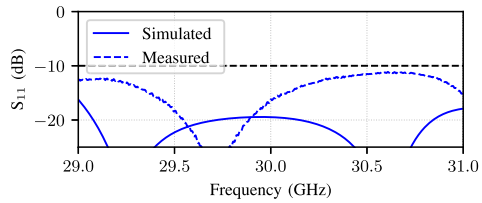

Fig. 8. Simulated and measured reflection coefficient of the prototype.

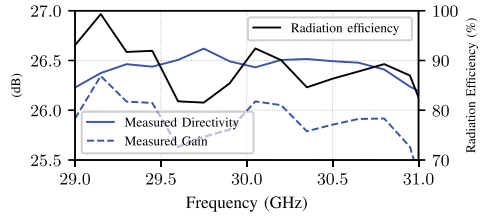

Fig. 9. Measured gain, directivity, and radiation efficiency.

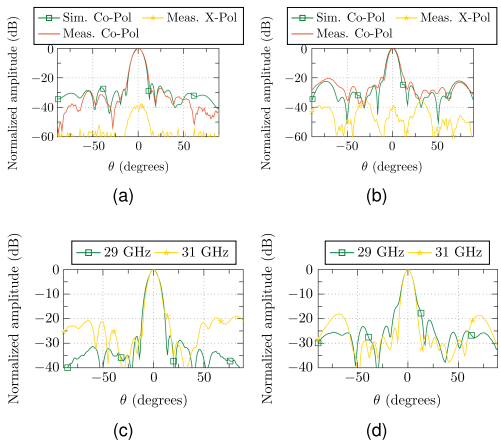

Fig. 10. (a) Measured normalized copolar and cross-polar radiation patterns at 30 GHz in *XZ*-plane and (b) in *YZ*-plane. Simulated normalized copolar also included. (c) Measured normalized copolar radiation patterns at 29 GHz and 31 GHz in *XZ*-plane and (d) in *YZ*-plane.

GHz to 31 GHz is shown. Fig. 9 illustrates the prototype's measured directivity, gain, and radiation efficiency across different frequencies. Notably, most of the band of interest exhibits a radiation efficiency above 85%. However, a slight reduction in this threshold is observed around a specific frequency (29.7 GHz). Nevertheless, overall, the antenna consistently maintains an efficiency level exceeding 82%. Fig. 10(a) and (b) depicts the simulated and measured co- and cross-polarized components in the *XZ*- and *YZ*-planes, corresponding to the E- and H-planes, respectively. A low SLL is found in the *XZ*-plane, better than -24.8 dB. The *YZ*-plane shows a slightly higher SLL than the *XY*-plane but is still below -20 dB. Both planes also have high cross-polarization discrimination, exceeding 40 dB in all planes, which is typical of rectangular slot arrays. Finally, Fig. 10(c) and (d) illustrates the copolarization pattern at the edges of the desired band (29 GHz and 31 GHz) in both main planes. It is important to note that the x-pol is intentionally omitted from the figures to enhance the clarity of the copolar patterns. The x-pol consistently performs better than -40 dB in both cases, as shown at the center frequency. Although the radiation patterns exhibit slight asymmetries, they are deemed acceptable and effectively fulfill the defined objectives. These asymmetries may stem from mutual couplings inherent in such a compact array, impacting the amplitude distribution. Nevertheless, the overall results remain highly satisfactory.

Finally, Table III shows key features of several antennas with low SLL available recently in the literature. The antenna demonstrates a significant improvement in efficiency, exceeding 82%, whereas the efficiencies of the antennas provided in Table III hover around 70%. Moreover, the proposed divider structure integrates naturally into the corporate feeding network, allowing for a very compact and simple design. Note that the proposed antenna requires only two pieces, keeping the antenna profile extremely low, below one λ_0. Other works with a low profile characteristic exist, but in exchange for lower efficiency due to the use of dielectric substrates. Also, [11] and [22] are GW-based antennas that also seek reduced SLL with Taylor distribution. Nevertheless, in these examples, an intermediate coupling layer is needed due to the feeding network bulkiness, and hence, slots are not fed individually but in groups of four slots. As a consequence, a quasi-Taylor amplitude distribution is synthesized with a noticeable impact on the radiation patterns.

V. CONCLUSION

In conclusion, the 8×8 Ka-band antenna design represents a significant breakthrough in high-gain metallic arrays. The antenna achieves a commendable SLL in both main planes by implementing a corporate feeding network with Taylor amplitude tapering. The proposed approach mitigates the inner coupling effects and maintains phase and amplitude stability across the radiating elements. Moreover, implementing a stepped transition elegantly aligns ridge heights, gradually decreasing toward the network end to enhance the coupling to the radiating slots and reducing the risk of interference. Despite its apparent ease, the key and novel contribution lies in its ability to create a very low-profile, entirely metallic antenna with highly compact splitters that can unbalance power distribution efficiently. It is verified that, to the best of the authors' best knowledge, this antenna exhibits the lowest layer requirement and superior radiation efficiency among antennas documented in the literature.

REFERENCES

[1] S. Chen, S. Sun, and S. Kang, "System integration of terrestrial mobile communication and satellite communication—the trends, challenges and key technologies in B5G and 6G," *China Commun.*, vol. 17, no. 12, pp. 156–171, 2020.

[2] M. K. Samimi and T. S. Rappaport, "3D millimeter-wave statistical channel model for 5G wireless system design," *IEEE Trans. Microw. Theory Techn.*, vol. 64, no. 7, pp. 2207–2225, Jul. 2016.

[3] A. Valero-Nogueira, E. Alfonso, J. I. Herranz, and P.-S. Kildal, "Experimental demonstration of local quasi-TEM gap modes in single-hard-wall waveguides," *IEEE Microw. Wireless Compon. Lett.*, vol. 19, no. 9, pp. 536–538, Sep. 2009.

[4] E. Alfonso, M. Baquero, P.-S. Kildal, A. Valero-Nogueira, E. Rajo-Iglesias, and J. I. Herranz, "Design of microwave circuits in ridge-gap waveguide technology," in *Proc. IEEE MTT-S Int. Microw. Symp.*, 2010, pp. 1544–1547.

[5] A. Jiménez Sáez, A. Valero-Nogueira, J. I. Herranz, and B. Bernardo, "Single-layer cavity-backed slot array fed by groove gap waveguide," *IEEE Antennas Wireless Propag. Lett.*, vol. 15, pp. 1402–1405, 2016.

[6] M. Ferrando-Rocher, A. Valero-Nogueira, and J. I. Herranz-Herruzo, "Exploring half-mode groove gap waveguide performance and advantages," in *Proc. 16th Eur. Conf. Antennas Propag.*, 2022, pp. 1–4.

[7] T. Taylor, "Design of line-source antennas for narrow beamwidth and low side lobes," *Trans. IRE Professional Group Antennas Propag.*, vol. 3, no. 1, pp. 16–28, 1955.

[8] H. A. Diawuo, S. J. Lee, and Y.-B. Jung, "Sidelobe-level reduction of a linear array using two amplitude tapering techniques," *Microw., Antennas Propag.*, vol. 11, no. 10, pp. 1432–1437, 2017.

[9] J. Vague et al., "Multipactor effect characterization of dielectric materials for space applications," *IEEE Trans. Microw. Theory Techn.*, vol. 66, no. 8, pp. 3644–3655, Aug. 2018.

[10] Z. Jiao, L. Jiang, J. Sun, J. Huang, and Y. Zhu, "Outgassing environment of spacecraft: An overview," *IOP Conf. Series: Mater. Sci. Eng.*, vol. 611, no. 1, 2019, Art. no. 012071.

[11] G.-L. Huang, S.-G. Zhou, T.-H. Chio, H.-T. Hui, and T.-S. Yeo, "A low profile and low sidelobe wideband slot antenna array fed by an amplitude-tapering waveguide feed-network," *IEEE Trans. Antennas Propag.*, vol. 63, no. 1, pp. 419–423, Jan. 2015.

[12] H. Li and Y. Li, "Low-sidelobe antenna array based on evanescent mode of cutoff waveguide," *IEEE Trans. Antennas Propag.*, vol. 70, no. 12, pp. 11608–11616, Dec. 2022.

[13] L. Qin, Y. Lu, Q. You, Y. Wang, J. Huang, and P. Gardner, "Millimeter-wave slotted waveguide array with unequal beamwidths and low sidelobe levels for vehicle radars and communications," *IEEE Trans. Veh. Technol.*, vol. 67, no. 11, pp. 10574–10582, Nov. 2018.

[14] P. Liu, G. F. Pedersen, and S. Zhang, "Wideband low-sidelobe slot array antenna with compact tapering feeding network for E-band wireless communications," *IEEE Trans. Antennas Propag.*, vol. 70, no. 4, pp. 2676–2685, Apr. 2022.

[15] X. Jiang et al., "Ka-band 8 x 8 low-sidelobe slot antenna array using a 1-to-64 high-efficiency network designed by new printed RGW technology," *IEEE Antennas Wireless Propag. Lett.*, vol. 18, no. 6, pp. 1248–1252, Jun. 2019.

[16] L. Li et al., "W-band ridge gap waveguide slot array antenna with low sidelobe and high-gain characteristics," *Microw. Opt. Technol. Lett.*, vol. 64, 2021.

[17] J. Ran, C. Jin, P. Zhang, W. Wang, and Y. Wu, "High-gain and low-loss dual-polarized antenna array with reduced sidelobe level based on gap waveguide at 28 GHz," *IEEE Antennas Wireless Propag. Lett.*, vol. 21, no. 5, pp. 1022–1026, May 2022.

[18] Y. Quan, J. Yang, H. Wang, and A. U. Zaman, "An unequal power divider based on ridge gap waveguide," in *Proc. 13th Eur. Conf. Antennas Propag.*, 2019, pp. 1–4.

[19] Z. Tao, Z. Peng, H. Yong, L. Xunxun, M. Yao, and L. Chao, "Design and fabrication of a high-gain low-sidelobe V-band wideband gap waveguide slot antenna array," in *Proc. 2nd China Int. SAR Symp.*, 2021, pp. 1–3.

[20] L. Li, C. Jin, B. Zhang, and P. Zhang, "E-band and low-sidelobe monopulse slot array antenna based on groove and ridge gap waveguide," in *Proc. IEEE MTT-S Int. Microw. Workshop Ser. Adv. Mater. Processes RF THz Appl.*, 2022, pp. 1–3.

[21] T. Li and Z. N. Chen, "Wideband sidelobe-level reduced ka-band metasurface antenna array fed by substrate-integrated gap waveguide using characteristic mode analysis," *IEEE Trans. Antennas Propag.*, vol. 68, no. 3, pp. 1356–1365, Mar. 2020.

[22] J. Liu, F. Yang, K. Fan, and C. Jin, "Unequal power divider based on inverted microstrip gap waveguide and its application for low sidelobe slot array antenna at 39 GHz," *IEEE Trans. Antennas Propag.*, vol. 69, no. 12, pp. 8415–8425, Dec. 2021.

[23] P. Kumar, A. Kedar, and A. K. Singh, "Design and development of low-cost low sidelobe level slotted waveguide antenna array in X-band," *IEEE Trans. Antennas Propag.*, vol. 63, no. 11, pp. 4723–4731, Nov. 2015.

[24] *IEEE Standard for Definitions of Terms for Antennas*, IEEE Std 145-2013 (Revision of IEEE Std 145-1993), pp. 1–50, 2014.